J. Fluid Mech. (1997), *vol.* 345, *pp.* 31–43. Printed in the United Kingdom

Thermocapillary convection in a cylindrical liquid-metal floating zone with a strong axial magnetic field and with a non-axisymmetric heat flux

By T. E. MORTHLAND AND J. S. WALKER

Department of Mechanical and Industrial Engineering, University of Illinois, Urbana, IL 61801, USA

(Received 24 June 1996 and in revised form 6 January 1997)

This paper treats the steady three-dimensional thermocapillary convection in a cylindrical liquid-metal zone between the isothermal ends of two coaxial solid cylinders and surrounded by an atmosphere. There is a uniform steady magnetic field which is parallel to the common centrelines of the liquid zone and solid cylinders, and there is a non-axisymmetric heat flux into the liquid's free surface. The magnetic field is sufficiently strong that inertial effects and convective heat transfer are negligible, and that viscous effects are confined to thin boundary layers adjacent to the free surface and to the liquid–solid interfaces. With an axisymmetric heat flux, the axisymmetric thermocapillary convection is confined to the thin layer adjacent to the free surface, but with a non-axisymmetric heat flux, there is an azimuthal flow inside the free-surface layer from the hot spot to the cold spot with the circulation completed by flow across the inviscid central core region. This problem is related to the magnetic damping of thermocapillary convection for the floating-zone growth of semiconductor crystals in Space.

1. Introduction

In the floating-zone process, a semiconductor crystal is grown from a volume of liquid (melt) which is held by surface tension between the growing cylindrical single crystal and the coaxial melting polycrystalline feed rod. A heat flux into the free surface keeps the melt temperature above the solidification temperature T_s. On Earth, only small-diameter crystals can be grown by the floating-zone process because surface tension can only balance the hydrostatic pressure variation for small zones (Coriell & Cordes 1977). With the heat flux provided by a single-loop radio-frequency induction coil around the melt, the electromagnetic (EM) body force in the skin-depth layer adjacent to the free surface augments the surface tension, so that larger crystals can be grown on Earth (Lie, Walker & Riahi 1990). However, this EM force also drives a strong circulation in the melt, leading to spatial oscillations in the crystal's dopant concentration, called striations (Muhlbauer, Erdmann & Keller 1983), where the dopant is added to give the semiconductor crystal the electrical properties needed for the integrated circuits to be manufactured on wafers sliced from the crystal. In an

Earth-orbiting vehicle, the residual acceleration is four or five orders of magnitude smaller than terrestrial gravity, so that large semiconductor crystals can be grown by the floating-zone process with nothing to augment the surface tension. The principal alternative for crystal growth in space is the Bridgman process in which the melt crystallizes inside a cylindrical ampoule, but stresses between the ampoule wall and the shrinking crystal can lead to surface dislocations in the crystal.

Since the surface tension of a liquid semiconductor decreases as the temperature is increased, surface-tension gradients drive a thermocapillary convection adjacent to the free surface from higher to lower temperatures. For the floating-zone growth of silicon or gallium-arsenide, the thermocapillary convection is periodic with temperature differences along the free surface of more than a few degrees Kelvin (Rupp *et al.* 1991), and this flow periodicity also produces the undesirable striations in the crystal. Numerical simulations (Muller & Rupp 1991; Rupp *et al.* 1991) and experiments (Croll, Dold & Benz 1994; Robertson & O'Connor 1986) have shown that a strong steady uniform axial magnetic field can eliminate or greatly reduce the unsteadiness in the thermocapillary convection and the resultant striations in the crystal for the temperature differences along the free surface of 10 to 30 K which occur in the actual process.

The furnace used for floating-zone crystal growth in space is an ellipsoid with a 1 kW lamp at one focal point and with the molten floating zone at the other focal point, so that the focused optical heating from the lamp keeps the temperature in the melt above T_s (Rupp *et al.* 1991). All previous treatments, including our studies (Morthland & Walker 1996, 1997), of thermocapillary convection in the floating-zone process with optical heating and with or without a steady magnetic field have assumed that the heat flux into the free surface is axisymmetric. In reality, the optical heat flux is never axisymmetric because the lamp may not be exactly at the focal point, the lamp itself is not axisymmetric, the axis of the crystal, feed rod and zone may not be perfectly aligned with the major axis of the ellipsoid, and an observation window has a much lower reflectivity than the metal surface so it produces a cold spot at its azimuthal position. Without a magnetic field, the relative deviation from axisymmetry in the melt motion is probably comparable to that in the heat flux. However, an axial magnetic field strongly suppresses an axisymmetric motion because there is very little electrical resistance to the azimuthal electric currents needed to provide the EM flow suppression, but an axial field only weakly suppresses azimuthal velocities near the free surface because the electrically insulating atmosphere blocks the radial electric currents needed for the EM body force opposing this velocity (Ma & Walker 1995). Therefore, with a strong axial magnetic field, a small deviation from axisymmetry in the heat flux can lead to a large deviation from axisymmetry in the melt motion. The results presented in this paper show that a deviation from axisymmetry leads to a fundamental change in the character of the flow. With an axisymmetric heat flux, the thermocapillary convection is confined to a boundary layer with an $O(Ha^{-1/2})$ dimensionless thickness adjacent to the free surface, where $Ha = BL(\sigma/\mu)^{1/2}$ is the large Hartmann number, B is the magnetic flux density of the externally applied steady uniform axial magnetic field and L is half the axial length of the free surface from the crystal to the feed rod, while σ and μ are the electrical conductivity and viscosity of the melt. In the rest of the melt, the velocity is zero to all orders in Ha. With a non-axisymmetric heat flux, there are large $O(Ha^{1/2})$ velocities in the free-surface layer from the hottest to the coldest azimuthal positions, while the circulation is completed by an $O(1)$ velocity across the central inviscid core region.

2. Problem formulation

The appropriate characteristic velocity for electromagnetically suppressed thermocapillary convection is $U = q(-\mathrm{d}\gamma/\mathrm{d}T^*)/Bk(\sigma\mu)^{1/2}$, where q is the characteristic magnitude of the heat flux into the free surface, $\mathrm{d}\gamma/\mathrm{d}T^*$ is the constant negative gradient of the surface tension γ with respect to the dimensional temperature T^*, and k is the melt's thermal conductivity (Khine & Walker 1994). In addition to the applied steady uniform axial magnetic field produced by a solenoid around the ellipsoidal furnace, there are 'induced' magnetic fields produced by the electric currents in the melt. The characteristic ratio of the induced to applied magnetic field strengths is the magnetic Reynolds number, $R_m = \mu_p \sigma U L$, where μ_p is the melt's magnetic permeability. Since R_m is very small for all crystal-growth processes, the induced magnetic fields are negligible. Therefore, the magnetic field normalized by B is simply $\hat{\boldsymbol{z}}$, where $\hat{\boldsymbol{r}}$, $\hat{\theta}$, $\hat{\boldsymbol{z}}$ are unit vectors for cylindrical coordinates with the z-axis along the common centrelines of the liquid zone and solid cylinders and with the origin midway between the ends of the cylinders.

The characteristic ratio of convective heat transfer to thermal conduction is the Péclet number, $Pe = \rho c_h UL/k$, where ρ and c_h are the melt's density and specific heat. With a sufficiently strong magnetic field U is small enough that $Pe \ll 1$ (Morthland & Walker 1997). Then the deviation of T^* from T_s, normalized by qL/k, is $T(r, \theta, z)$ which is governed by $\nabla^2 T = 0$. In the Navier–Stokes equation, the characteristic ratio of the EM body force term to the inertial terms is the interaction parameter, $N = \sigma B^2 L/\rho U$, which varies as B^3 for our U. Since our solution involves large, $O(Ha^{1/2})$, dimensionless velocities in a free-surface layer with an $O(Ha^{-1/2})$ dimensionless thickness, N must be much larger than $Ha^{3/2}$ in order to neglect inertial effects (Walker, Ludford & Hunt 1972). With these assumptions, the dimensionless governing equations are

$$0 = -\boldsymbol{\nabla} p + \boldsymbol{j} \times \hat{\boldsymbol{z}} + Ha^{-2}\nabla^2 \boldsymbol{v}, \quad \boldsymbol{\nabla}\cdot\boldsymbol{v} = 0, \tag{1a, b}$$

$$\boldsymbol{j} = -\boldsymbol{\nabla}\phi + \boldsymbol{v} \times \hat{\boldsymbol{z}}, \qquad \boldsymbol{\nabla}\cdot\boldsymbol{j} = 0, \tag{1c, d}$$

where p, $\boldsymbol{j}$, $\boldsymbol{v}$ and ϕ are the pressure, electric current density, velocity and electric potential function (voltage), normalized by $\sigma U B^2 L$, $\sigma U B$, U and UBL, respectively.

We neglect the small electrical conductivity of the feed rod and crystal, so that the boundary conditions at the liquid–solid interfaces are

$$\boldsymbol{v} = 0, \quad j_z = 0 \quad \text{at} \quad z = \pm 1. \tag{2}$$

For terrestrial floating-zone crystal growth, the free surface is far from cylindrical because surface tension must balance the hydrostatic pressure variation (Coriell & Cordes 1977). In Space, with a negligible hydrostatic pressure variation due to the small residual acceleration, the free-surface shape is very close to a cylinder (Morthland & Walker 1996), and the free-surface distortion produced by the pressure variation associated with the melt motion is negligible (Lie *et al.* 1990). Therefore the boundary conditions at the free surface are

$$v_r = 0, \quad \frac{\partial v_\theta}{\partial r} - \frac{v_\theta}{a} = -\frac{Ha}{a}\frac{\partial T}{\partial \theta}, \tag{3a, b}$$

$$\frac{\partial v_z}{\partial r} = -Ha\frac{\partial T}{\partial z}, \quad j_r = 0 \quad \text{at} \quad r = a, \tag{3c, d}$$

where a is the ratio of the floating zone's diameter to its axial length $2L$. If the heat flux into the free surface is symmetric about the $z = 0$ plane, then the melt motion is too,

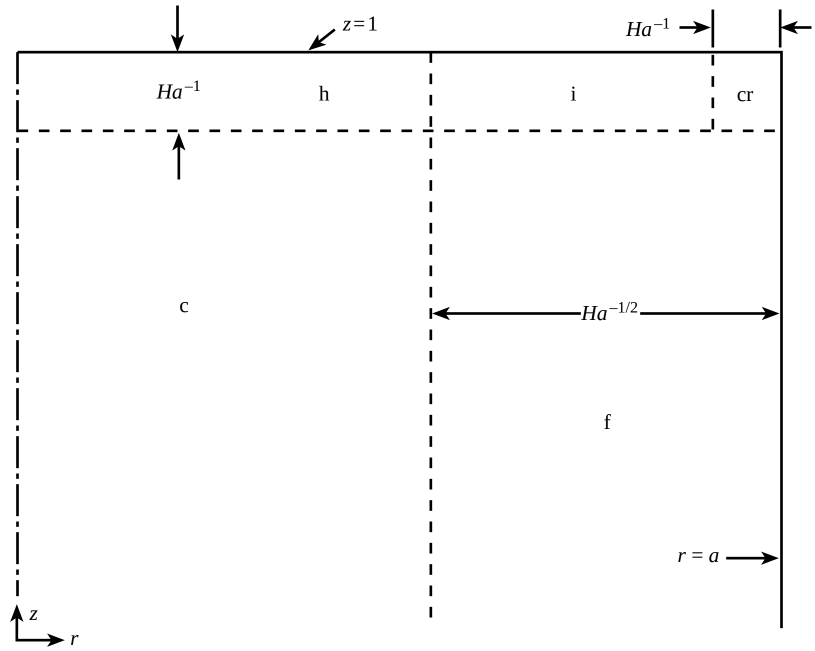

FIGURE 1. Subregions of the liquid zone for $Ha \gg 1$ and for $z > 0$: c = inviscid core region, h = Hartmann layer, f = free-surface layer, i = intersection region and cr = corner region.

so that we need only solve for $0 \leqslant z \leqslant 1$, with appropriate symmetry conditions at $z = 0$. We make p and ϕ unique by setting $p = \phi = 0$ at $r = z = 0$.

For $Ha \gg 1$, the liquid zone can be divided into the subregions shown in figure 1. The Hartmann-layer solution satisfies (2) and matches the core solution, provided the latter satisfies the Hartmann conditions

$$v_{zc} = -Ha^{-1} r^{-1} \left[\frac{\partial}{\partial r}(r v_{rc}) + \frac{\partial v_{\theta c}}{\partial \theta} \right], \tag{4a}$$

$$j_{zc} = Ha^{-1} r^{-1} \left[\frac{\partial v_{rc}}{\partial \theta} - \frac{\partial}{\partial r}(r v_{\theta c}) \right] \quad \text{at} \quad z = 1, \tag{4b}$$

neglecting $O(Ha^{-2})$ terms (Walker *et al.* 1972), where the subscript c denotes a core variable. The solution of (1) which satisfies (4) is

$$j_{rc} = -\frac{1}{r}\frac{\partial p_c}{\partial \theta}, \quad j_{\theta c} = \frac{\partial p_c}{\partial r}, \quad j_{zc} = 0, \tag{5a–c}$$

$$v_{rc} = -\frac{1}{r}\frac{\partial \phi_c}{\partial \theta} - \frac{\partial p_c}{\partial r}, \quad v_{zc} = 0, \tag{5d, e}$$

$$v_{\theta c} = \frac{\partial \phi_c}{\partial r} - \frac{1}{r}\frac{\partial p_c}{\partial \theta}, \tag{5f}$$

neglecting $O(Ha^{-1})$ terms, where $p_c(r, \theta)$ and $\phi_c(r, \theta)$ satisfy $\nabla^2 p_c = \nabla^2 \phi_c = 0$. In the present problem, the $O(Ha^{-1})$ term on the right-hand side of (4b) is needed in order to determine the equation governing the $O(1)$ ϕ_c (Hunt & Ludford 1968), while the $O(Ha^{-1})$ term on the right-hand side of (4a) plays no role. In other applications, the $O(Ha^{-1})$ term on the right-hand side of (4a) plays the key role when the Hartmann-layer pumping drives the core flow (Hall & Walker 1993). The boundary conditions on p_c and ϕ_c at $r = a$ are obtained by matching the free-surface-layer solution, while $p_c = \phi_c = 0$ at $r = 0$.

For the free-surface layer, we stretch the local radial coordinate by introducing $\xi = Ha^{1/2}(r-a)$. With the subscript f denoting the leading-order term in the asymptotic expansion of a free-surface-layer variable then: $v_{\theta f}$ and v_{zf} are $O(Ha^{1/2})$; v_{rf}, $j_{\theta f}$, j_{zf} and ϕ_f are $O(1)$; j_{rf}, p_f and an integration function F_f are $O(Ha^{-1/2})$. The leading-order terms in (1) give expressions for the other variables in terms of ϕ_f and F_f, and give the equations governing ϕ_f and F_f:

$$v_{rf} = -\frac{1}{a}\frac{\partial \phi_f}{\partial \theta} - \frac{\partial^2 F_f}{\partial \xi\, \partial z}, \quad v_{\theta f} = \frac{\partial \phi_f}{\partial \xi}, \tag{6a, b}$$

$$j_{rf} = \frac{\partial^3 \phi_f}{\partial \xi^3} - \frac{1}{a}\frac{\partial^2 F_f}{\partial \theta\, \partial z}, \quad j_{\theta f} = \frac{\partial^2 F_f}{\partial \xi\, \partial z}, \tag{6c, d}$$

$$v_{zf} = \frac{\partial^2 F_f}{\partial \xi^2}, \quad j_{zf} = -\frac{\partial \phi_f}{\partial z}, \quad p_f = \frac{\partial F_f}{\partial z}, \tag{6e–g}$$

$$\frac{\partial^2 \phi_f}{\partial z^2} = \frac{\partial^4 \phi_f}{\partial \xi^4}, \quad \frac{\partial^2 F_f}{\partial z^2} = \frac{\partial^4 F_f}{\partial \xi^4}. \tag{6h, i}$$

The free-surface conditions (3) become

$$\frac{\partial^2 \phi_f}{\partial \xi^2} = -\frac{1}{a}\frac{\partial T}{\partial \theta}(a, \theta, z), \quad \frac{\partial^3 F_f}{\partial \xi^3} = -\frac{\partial T}{\partial z}(a, \theta, z), \tag{7a, b}$$

$$\frac{\partial^2 F_f}{\partial \xi\, \partial z} + \frac{1}{a}\frac{\partial \phi_f}{\partial \theta} = 0, \quad \frac{\partial^3 \phi_f}{\partial \xi^3} - \frac{1}{a}\frac{\partial^2 F_f}{\partial \theta\, \partial z} = 0 \quad at \quad \xi = 0. \tag{7c, d}$$

The intersection-region solution satisfies (2) and matches the free-surface-layer solution, provided the latter satisfies the Hartmann conditions (Walker *et al.* 1972)

$$\frac{\partial^2 F_f}{\partial \xi^2} = 0, \quad \frac{\partial \phi_f}{\partial z} = \frac{\partial^2 \phi_f}{\partial \xi^2} \quad \text{at} \quad z = 1. \tag{8a, b}$$

Since the free-surface-layer pressure is $O(Ha^{-1/2})$, the $O(1)$ core pressure is zero at $r = a$, so that it is zero everywhere. With the subscript c denoting the leading-order term in the asymptotic expansion of a core variable, v_{rc}, $v_{\theta c}$ and ϕ_c are $O(1)$, while j_{rc}, $j_{\theta c}$ and p_c are $O(Ha^{-1/2})$, and the terms with p_c in (5d) and (5f) are eliminated. Matching the core solution gives the conditions

$$\phi_f \to \phi_c(a, \theta), \quad F_f \to z p_c(a, \theta) \quad \text{as} \quad \xi \to -\infty, \tag{9a, b}$$

so that (8a) can be replaced by $F_f(\xi, \theta, 1) = p_c(a, \theta)$. F_f and ϕ_f are odd and even functions of z, respectively. In the next Section, we present solutions for a specific distribution of the heat flux into the free surface.

The present neglect of convective heat transfer everywhere, inertial effects everywhere and viscous effects in the core assumes that the respective parameters $Pe\, Ha^{-1/4}$, $N^{-1}\, Ha^{3/2}$ and $Ha^{-1/2}$ are small (Morthland & Walker 1997). As an example, we consider the properties of molten silicon (Sabhapathy & Salcudean 1991), a floating-zone axial length of 1 cm, and a temperature difference along the free surface of 15 K (Croll *et al.* 1994), so that $Ha = 207B$, $N = 81.83B^3$ and $Pe = 6.79B^{-1}$. For the $B = 0.5$ T used by Croll *et al.* (1994), $Pe\, Ha^{-1/4} = 4.257$, $N^{-1}\, Ha^{3/2} = 103$, and $Ha^{-1/2} = 0.1$. For this case, convective heat transfer and inertial effects are clearly not negligible, and the present assumptions are not appropriate. Indeed the experiments of Croll *et al.* (1994) showed that an instability leads to a periodic flow which produces striations in the part of the crystal adjacent to the free-surface layer. Smith & Davis (1983) showed that such an instability involves a coupling of convective heat transfer and inertial effects which produces hydrothermal waves propagating around the floating zone in the azimuthal direction. In order to eliminate these undesirable striations, researchers at the NASA Marshall Space Flight Center and at the University of Freiburg are collaborating to grow silicon crystals with the same floating-zone process used by Croll *et al.* (1994), but with $B = 5$ T. For this magnetic flux density, the present assumptions are certainly appropriate. For these terrestrial experiments, the deviation from a cylindrical free surface will be small because the radius of the floating zone will be small. The model presented in this paper should help explain the results of these planned experiments.

All of the orders of magnitude in $Ha^{-1/2}$ follow from our characteristic melt velocity U, which was chosen to give $O(1)$ dimensionless volumetric flow rates, i.e. flow rates which remain bounded and non-zero as $Ha \to \infty$. The two temperature gradients driving the flow are the $\partial T/\partial\theta$ and $\partial T/\partial z$ in (3b, c). Since $\partial/\partial\theta$ and $\partial/\partial z$ are $O(1)$, while $\partial/\partial r$ is $O(Ha^{1/2})$ in the free-surface layer, (3c) implies that v_z is always $O(Ha^{1/2})$ inside this layer, and (3b) implies that v_θ is $O(Ha^{1/2})$ inside this layer when $\partial T/\partial\theta$ is not zero. Since these large velocities are tangential velocities inside a layer with an $O(Ha^{-1/2})$ thickness, they represent $O(1)$ dimensionless flow rates. The axisymmetric flow is entirely confined to the free-surface layer, but any deviation from axisymmetry requires that the flow circuit be completed across the core, which implies $O(1)$ core velocities. The electric current arises from the large velocities in the free-surface layer, and each component of $\boldsymbol{j}$ in this layer is $O(Ha^{-1/2})$ smaller than the corresponding component of $\boldsymbol{v}$. The $O(Ha^{-1/2})$ current across the core arises from the need to complete the electrical circuit for the free-surface-layer currents.

3. Axisymmetric and non-axisymmetric solutions

The derivatives of $T(a,\theta,z)$ in (7a) and (7b) are the only inhomogeneous terms in the linear problem (6)–(9). Since the Fourier components in θ are decoupled, we can illustrate the effects of a non-axisymmetric heat flux with only the first two Fourier components, namely 1 and $\cos\theta$. For simplicity, we assume that the axial variation of the heat flux is given by $\cos(\frac{1}{2}\pi z)$, so that the separation-of-variables solution for T has only one term. The boundary conditions on T are

$$\frac{\partial T}{\partial r} = \cos(\tfrac{1}{2}\pi z)\,[1+\lambda\cos\theta] \quad \text{at} \quad r = a, \tag{10a}$$

$$T = 0 \quad \text{at} \quad z = \pm 1, \tag{10b}$$

where the parameter λ reflects the relative deviation from axisymmetry, i.e. the dimensional heat flux at $z = 0$ varies from a maximum of $(1+\lambda)\,q$ at $\theta = 0$ to a minimum of $(1-\lambda)\,q$ at $\theta = \pm\pi$, while (10b) reflects the fact that $T^* = T_s$ at the melting feed-rod surface and at the solidifying crystal surface. The solution for T is

$$T = \cos(\tfrac{1}{2}\pi z)\left\{\frac{2}{\pi}I_0(\tfrac{1}{2}\pi r)\,[I_1(\tfrac{1}{2}\pi a)]^{-1} + \lambda\cos\theta I_1(\tfrac{1}{2}\pi r)\,[\tfrac{1}{2}\pi\, I_0(\tfrac{1}{2}\pi a) - a^{-1}I_1(\tfrac{1}{2}\pi a)]^{-1}\right\}, \tag{11}$$

where I_0 and I_1 are the modified Bessel functions of the first kind and zeroth or first order.

In both the core and the free-surface layer, p, v_r, v_z, j_θ and F_f have the form $p = p_a + \lambda \cos\theta p_n$, while ϕ, v_θ, j_r and j_z have the form $\phi = \lambda \sin\theta \phi_n$, where the subscript a denotes the axisymmetric melt motion with $\phi = v_\theta = j_r = j_z = 0$, the subscript n denotes the non-axisymmetric melt motion which is superimposed on the axisymmetric one, and variables with the subscript a or n are functions of r in the core and of ξ and z in the free-surface layer.

For the axisymmetric flow, $\phi_{ca} = p_{ca} = 0$, so that all the core variables are zero. Indeed, it is easy to show that all the core variables are zero to all order in Ha for the axisymmetric flow. In the free-surface layer, the separation-of-variables solution for F_{fa} is

$$F_{fa} = -\pi^{-2} I_0(\tfrac{1}{2}\pi a)\,[I_1(\tfrac{1}{2}\pi a)]^{-1} \times \sum_{k=1}^{\infty} (-1)^k \gamma_k^{-1}(k^2-\tfrac{1}{4})^{-1} \sin(k\pi z)\exp(\gamma_k \xi)\,[\sin(\gamma_k \xi) - \cos(\gamma_k \xi)], \quad (12)$$

where $\gamma_k = (\tfrac{1}{2}k\pi)^{1/2}$.

For the non-axisymmetric flow, the core solution is $\phi_{cn} = C_1 r$ and $p_{cn} = C_2 r$, where the constants C_1 and C_2 will be determined in the solution for the free-surface layer. In Cartesian coordinates with the x- and y-axes parallel to the $\theta = 0$ and $\theta = \tfrac{1}{2}\pi$ radii, respectively, (5) gives

$$v_x = -C_1\lambda, \quad v_y = 0, \quad j_x = 0, \quad j_y = C_2\lambda Ha^{-1/2}, \qquad (13\,a\text{–}d)$$

in the core, where (13a) and (13b) neglect $O(Ha^{-1/2})$ terms, while (13c) and (13d) neglect $O(Ha^{-1})$ terms. Since C_1 and C_2 both turn out to be negative, there is a uniform $O(1)$ velocity across the core from the cold side for $|\theta| > \tfrac{1}{2}\pi$ to the hot side for $|\theta| < \tfrac{1}{2}\pi$, and this flow drives a uniform $O(Ha^{-1/2})$ electric current from $0 < \theta < \pi$ to $-\pi < \theta < 0$. The uniformity of the core velocity and current follows from only including $\cos\theta$ – the $\cos 2\theta$ term would involve a non-uniform core velocity from $\theta = \pm\tfrac{1}{2}\pi$ to $\theta = 0$ and $\theta = \pi$, etc.

In the free-surface layer, ϕ_{fn} and F_{fn} are governed by (6h) and (6i). In the free-surface conditions (7), the right-hand sides of (7a) and (7b) are replaced by

$$\frac{Q}{a}\cos(\tfrac{1}{2}\pi z), \quad \tfrac{1}{2}\pi\, Q\, sin(\tfrac{1}{2}\pi z), \qquad (14\,a, b)$$

respectively, where

$$Q = I_1(\tfrac{1}{2}\pi a)\,[\tfrac{1}{2}\pi\, I_0(\tfrac{1}{2}\pi a) - a^{-1} I_1(\tfrac{1}{2}\pi a)]^{-1}, \qquad (14\,c)$$

while the $\partial/\partial\theta$ in (7c) and (7d) is replaced by $+1$ and -1, respectively. ϕ_{fn} satisfies (8b), and

$$F_{fn} = C_2 a \quad \text{at} \quad z = 1, \qquad (15)$$

while (9) become

$$\phi_{fn} \to C_1 a, \quad F_{fn} \to C_2 az \quad \text{as} \quad \xi \to -\infty. \qquad (16\,a, b)$$

The separation-of-variables solution for (6i), (7b) with (14b), (15) and (16b) is

$$F_{fn} = C_2 az + \sum_{k=1}^{\infty} \sin(k\pi z)\exp(\gamma_k \xi)\{A_k[\sin(\gamma_k \xi) + \cos(\gamma_k \xi)] + Q(-1)^k[\pi\gamma_k(k^2-\tfrac{1}{4})]^{-1}\cos(\gamma_k \xi)\}, \quad (17)$$

where the coefficients A_k will be determined by (7c) and (7d). For ϕ_{fn}, (8b) precludes a separation-of-variables solution, so we used a Fourier sine transform (Walker *et al.* 1972) to solve (6h), (7a) with (14a), and (8b), and excluding exponential growth,

$$\phi_{fn}(\xi,z) = \frac{1}{2}\int_{-1}^{z}\left[\frac{Q}{a}\cos\left(\tfrac{1}{2}\pi z^*\right)+\frac{\partial\phi_{fn}}{\partial z}(0,z^*)\right]\operatorname{erf}\left[\tfrac{1}{2}\xi(z-z^*)^{-1/2}\right]\mathrm{d}z^* + \frac{1}{2}\int_{z}^{1}\left[\frac{Q}{a}\cos\left(\tfrac{1}{2}\pi z^*\right)-\frac{\partial\phi_{fn}}{\partial z}(0,z^*)\right]\operatorname{erf}\left[\tfrac{1}{2}\xi(z^*-z)^{-1/2}\right]\mathrm{d}z^* + \phi_{fn}(0,z). \tag{18}$$

The values of $\phi_{fn}(0,z)$ will also be determined by (7c) and (7d).

C_1 is determined by (16a) and (18):

$$C_1 = a^{-1}\phi_{fn}(0,+1) - 2\pi^{-1}a^{-2}Q. \tag{19}$$

Equation (18) cannot be introduced directly into (7d) because the integrand at $\xi = 0$ would be too singular at $z^* = z$, so that we integrated (18) by parts with respect to z^* before differentiating thrice with respect to ξ and setting $\xi = 0$ for (7d). With (17) and (18), (7d) becomes a singular Fredholm integral equation for the values of $\partial^2\phi_{fn}/\partial z^2(0,z^*)$, and also involves a Fourier series with the coefficients A_k. The series in (7d) involves $\cos(k\pi z)$, beginning with $k=1$, so that the integral of (7d) from $z=0$ to $z=1$ gives

$$C_2 = \pi^{-1/2}\int_{-1}^{1}\left[\frac{\pi Q}{2a}\sin\left(\tfrac{1}{2}\pi z^*\right)-\frac{\partial^2\phi_{fn}}{\partial z^2}(0,z^*)\right](1-z^*)^{1/2}\,\mathrm{d}z^* + \left(\frac{2}{\pi}\right)^{1/2}\frac{\partial\phi_{fn}}{\partial z}(0,+1). \tag{20}$$

We introduced (17) and (18) into (7c), multiplied by $\cos(m\pi z)$, and integrated from $z=0$ to $z=1$. For $m=0$, (7c) gives

$$\int_{0}^{1}\phi_{fn}(0,z)\,\mathrm{d}z = 0, \tag{21}$$

so that the values of $\phi_{fn}(0,z)$ and $\partial\phi_{fn}/\partial z(0,z)$ are easy to obtain from the values of $\partial^2\phi_{fn}/\partial z^2(0,z)$. For $m = 1,2,3,\ldots$, (7c) gives

$$\int_{0}^{1}\frac{\partial^2\phi_{fn}}{\partial z^2}(0,z^*)\left[(-1)^m-\cos(m\pi z^*)\right]\mathrm{d}z^* + a\pi^3 m^3\gamma_m A_m = -\tfrac{1}{2}aQ(-1)^m\pi^2 m^3\left(m^2-\tfrac{1}{4}\right)^{-1}. \tag{22}$$

Equations (7d) and (22) are a pair of equations for $\partial^2\phi_{fn}/\partial z^2(0,z^*)$ and A_k. We divided the interval $0 \leqslant z \leqslant 1$ into NZ segments, with the ends of the segments at the Gauss–Lobatto points, $z_n = \cos(n\pi/2NZ)$ for $n=0$ to NZ, so that the segments are short and long near $z=1$ and $z=0$ where the gradient of $\partial^2\phi_{fn}/\partial z^2(0,z^*)$ is large and small, respectively. We assumed that the value of $\partial^2\phi_{fn}/\partial z^2(0,z^*)$ is constant over each segment, giving NZ discrete unknown values of this function. Equation (7d) was evaluated at the centre of each segment giving NZ equations for the NZ unknown values of $\partial^2\phi_{fn}/\partial z^2(0,z^*)$ and for A_k. The Fourier series in (7d) was truncated at $k = NA$ and (22) was used for $m=1$ to NA, giving a total of $(NZ+NA)$ simultaneous linear algebraic equations for the $(NZ+NA)$ unknown. Varying NZ and NA indicated that $NZ = NA = 40$ gives excellent results. The values of the free-surface-layer variables are given by (6a–g), (17) truncated at $k = NA$, and (18) with the constant values of $\partial^2\phi_{fn}/\partial z^2(0,z^*)$ for each segment; while C_1 and C_2 are given by (19) and (20).

4. Results

Here we only present results for $a = 1$. For the axisymmetric flow inside the free-surface layer, there is a stream function, but the contours of v_{rfa} and v_{zfa} in figure 2 are more useful than the streamlines for comparing the axisymmetric and non-

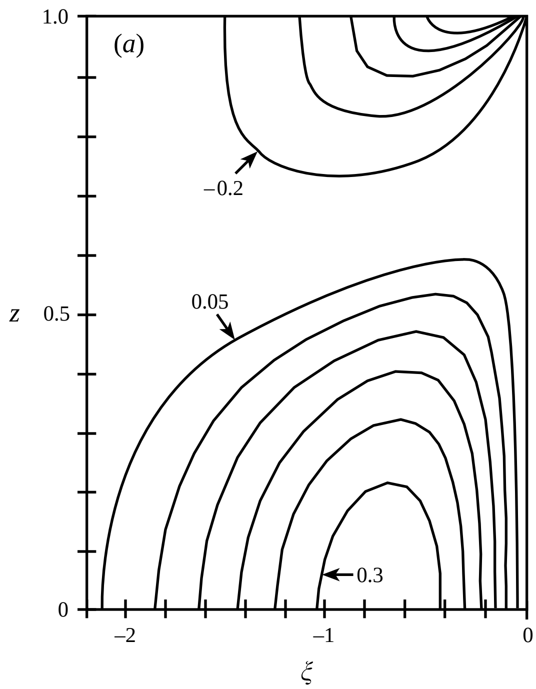

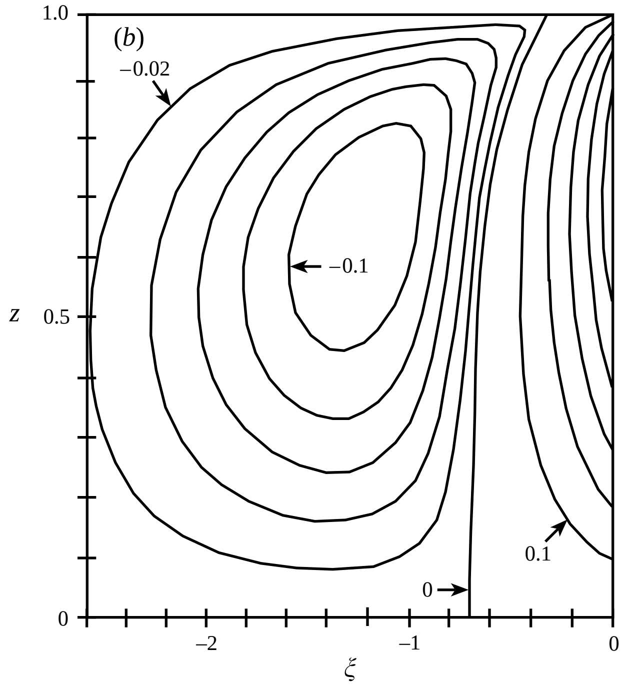

FIGURE 2. Contours of the velocity components for the axisymmetric flow inside the free-surface layer. (*a*) $v_{rfa} = -0.2n$ for $n = 1$ to 5 and $v_{rfa} = 0.05n$ for $n = 1$ to 6. (*b*) $v_{zfa} = -0.02n$ for $n = 1$ to 5 and $v_{zfa} = 0.1n$ for $n = 1$ to 5.

axisymmetric flows. In figure 2, the velocity differences between adjacent contours are different for positive and negative values. Here $-1.26 < v_{rfa} < 0.341$, and $-0.118 < v_{zfa} < 0.561$. For the axisymmetric flow, the melt near the free surface flows toward each solid–liquid interface, turns to flow radially inward with a large velocity near the interface, flows back toward $z = 0$ for $\xi < -0.7$ and then flows radially outward toward the free surface for $|z| < 0.6$. These results agree with the axisymmetric results presented by Morthland & Walker (1997).

While v_{rfa} and v_{zfa} are both zero at $\xi = 0$ and $z = 1$, figures 2(*a*) and 2(*b*) show that $\partial v_{rfa}/\partial \xi$ and $\partial v_{zfa}/\partial z$ have singularities at this corner. These singularities arise because $v_{zfa} = 0$ at $z = 1$ for all ξ, while $\partial v_{zfa}/\partial \xi$ at $\xi = 0$ approaches its maximum value as $z \to 1$. The solution of the parabolic equation (6*i*) which satisfies these incompatible boundary conditions has the local behaviour

$$\frac{\partial v_{zfa}}{\partial \xi} \approx I_0(\tfrac{1}{2}\pi a)\,[I_1(\tfrac{1}{2}\pi a)]^{-1}\left\{1+\operatorname{erf}\left[\frac{\xi}{2(1-z)^{1/2}}\right]\right\}. \tag{23}$$

For the corner region (cr) in figure 1, $\Delta r = O(Ha^{-1})$, $\Delta z = O(Ha^{-1})$, and the governing equation is elliptic. The corner-region solution matches the singularities in the free-surface-layer velocity gradients at $\xi = 0$ and $z = 1$. The axial temperature gradient accelerates the flow along the free surface from the plane of symmetry at $z = 0$ toward the solid surface at $z = 1$. In the free-surface layer, the viscous momentum diffusion in the z-direction is negligible, so that nothing decelerates the flow until it is very close to the solid surface. Very near $z = 1$, the flow abruptly turns radially inward, creating an abrupt decrease in v_{rfa} from zero as ξ decreases from zero. The infinite velocity gradients are resolved by the smaller scales of the corner region where all viscous effects are important. As always, there are no infinite velocity gradients at the physical scale of the viscous diffusion length, which is Ha^{-1} here, but there appear to be infinite velocity gradients when we study scales which are much larger than the viscous diffusion length.

For the non-axisymmetric flow, $C_1 = -0.388$ and $C_2 = -0.268$. The contours of v_{rfn}, $v_{\theta fn}$ and v_{zfn} are presented in figure 3. Again there are singularities in the gradients of v_{rfn} and v_{zfn}. In addition there are new singularities in j_{rfn} and j_{zfn} at $\xi = 0$ and $z = 1$. The total radial electric current inside the intersection region (i) in figure 1 at any value of ξ is proportional to the local value of $v_{\theta fn}$ at $z = 1$. Figure 3(*b*) shows that $v_{\theta fn}$ is not zero at $\xi = 0$ and $z = 1$, so that there is a non-zero radial electric current from the intersection region to the corner region. Continuity of electric current requires that this current in turn enter the free-surface layer as an apparent current source at $\xi = 0$ and $z = 1$. Indeed this current flows out of the corner region and into the free-surface layer along the parabolas defined by $\xi/(1-z)^{1/2} = \text{constant}$.

Here $-0.723 < v_{rfn} < 0.502$, $0 < v_{\theta fn} < 0.539$, and $-0.0715 < v_{zfn} < 0.351$. The values of $v_{rfn}(\xi, z)$ and $v_{zfn}(\xi, z)$ are multiplied by $\cos\theta$, while the values of $v_{\theta fn}$ are multiplied by $\sin\theta$. The non-axisymmetric flow consists of a planar flow in $\theta =$ constant planes and a nearly planar flow which only moves slightly across $z =$ constant planes. The flow in $\theta =$ constant planes is confined to the free-surface layer and increases or decreases the axisymmetric flow on the hot side for $|\theta| < \frac{1}{2}\pi$ or on the cold side for $|\theta| > \frac{1}{2}\pi$, respectively. Most of v_{zfn} in figure 3(*c*) is in this planar flow. The maximum values of v_{zfa} and v_{zfn} both occur at $\xi = 0$ near $z = 0.7$, so that the maximum axial-free-surface velocity at each azimuthal position is $(0.561 + 0.351\lambda\cos\theta)$.

The other part of the non-axisymmetric flow consists of the uniform velocity $v_x = 0.388\lambda$ across the core from the cold side to the hot side and an azimuthal velocity inside the free-surface layer from the hot side to the cold side. In figure 3(*b*) $v_{\theta fn}$ is the

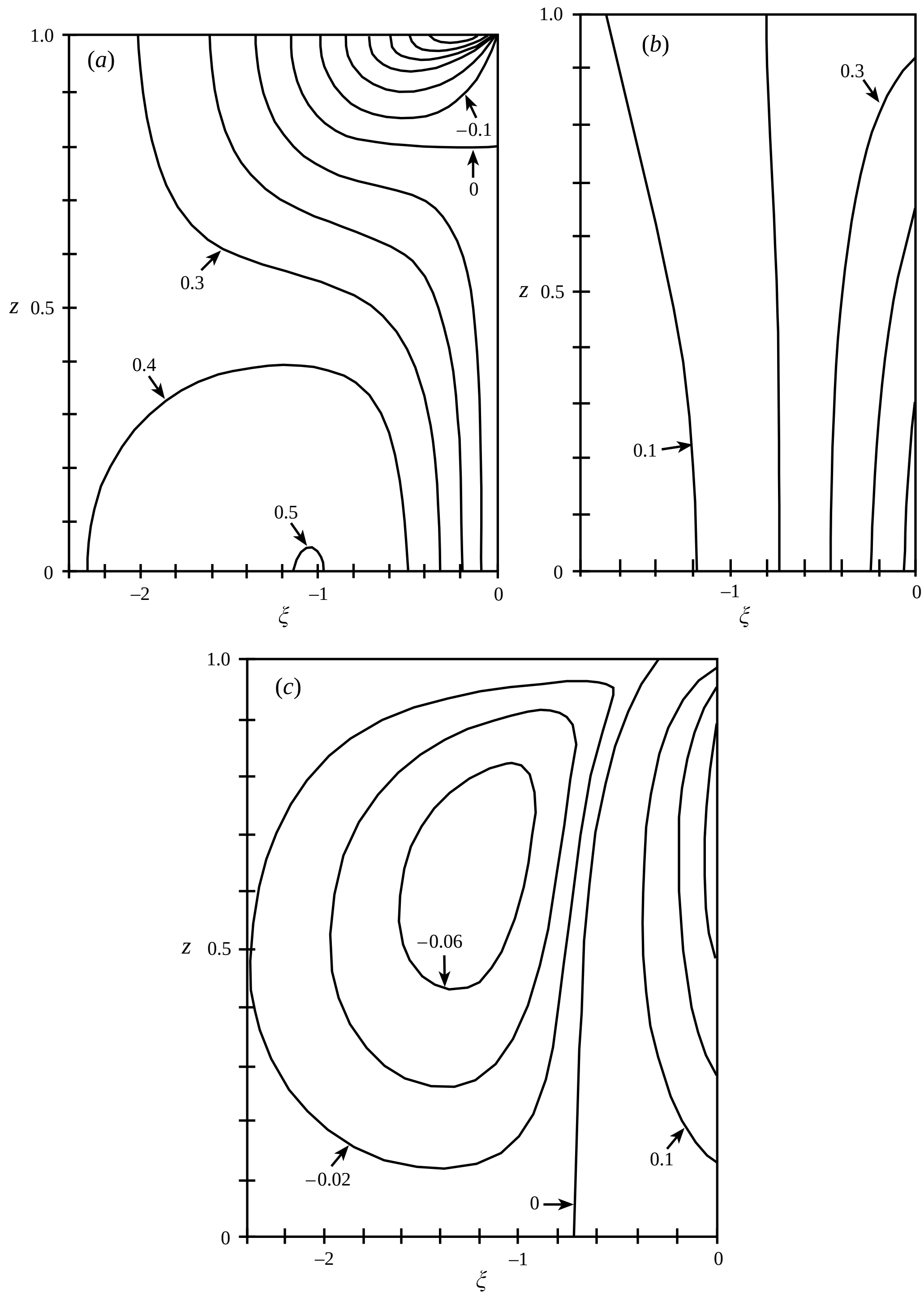

FIGURE 3. Contours of the velocity components for the non-axisymmetric flow inside the free-surface layer. (*a*) $v_{rfn} = 0.1n$ for $n = -6$ to 5. (*b*) $v_{\theta fn} = 0.1n$ for $n = 1$ to 5. (*c*) $v_{zfn} = -0.02n$ for $n = 1$ to 3 and $v_{zfn} = 0.1n$ for $n = 0$ to 3.

azimuthal velocity inside the free-surface layer and is nearly uniform in z, like the core velocity. The integral of $v_{\theta fn}$ from $\xi = -\infty$ to $\xi = 0$ varies from 0.376 at $z = 0$ to 0.408 at $z = 1$, so that a small part of the v_{zfn} in figure 3(c) provides an axial redistribution between the uniform core flow and the azimuthal flow inside the free-surface layer which is slightly stronger near the liquid–solid interfaces. In figure 3(a) v_{rfn} represents a superposition of the two parts of the non-axisymmetric flow. For the part in $\theta =$ constant planes, v_{rfn} is positive and negative near $z = 0$ and $z = 1$, respectively. For the part which nearly lies in $z =$ constant planes, v_{rfn} decreases from 0.388 at $\xi = -\infty$ to zero at $\xi = 0$.

5. Conclusions

The thermocapillary convection in a cylindrical floating zone with a strong uniform axial magnetic field and with an axisymmetric heat flux into the free surface represents a special case in which the strong electromagnetic suppression of the motion completely eliminates all melt motion in the central core region, leaving only the circulation in the azimuthal planes inside a thin boundary layer adjacent to the free surface. If there is a deviation from axisymmetry in the heat flux, the azimuthal variation of the temperature around the free surface drives an azimuthal velocity inside the free-surface layer from the hot side to the cold side, and the circulation is completed by a velocity across the central core of the melt from the cold side to the hot side. This transverse flow across the entire face of the growing crystal could produce a variation of the dopant concentration across each cross-section of the crystal or lateral macro-segregation.

We can expect the transverse core flow driven by a deviation from axisymmetry in the heat flux to affect the distribution of a dopant in the crystal when the mass-transport Péclet number based on the core velocity is greater than 1, i.e.

$$Pe_m = \frac{(-C_1 \lambda U) L}{D} > 1, \tag{24}$$

where D is the diffusion coefficient for the dopant in the molten semiconductor. Using the properties of molten silicon, a zone length of 1.0 cm, a free-surface temperature difference of 15 K, $B = 5.0$ T and the typical value $D = 10^{-8}$ m^2 s^{-1}, (24) implies a significant effect for $\lambda > 0.0089$. Therefore we can expect that even a small deviation from axisymmetry will have a significant effect on the dopant distribution.

Here we have only considered a relative deviation from an axisymmetric heat flux given by $\lambda \cos\theta$, i.e. the hottest and coldest azimuthal positions at $\theta = 0$ and $\theta = \pi$, respectively. Certain floating-zone furnaces use two lamps placed diametrically opposite each other, so that the relative deviation from an axisymmetric heat flux will be given by $\lambda \cos(2\theta)$, with the hottest positions at $\theta = 0, \pi$ and the coldest positions at $\theta = \pm\frac{1}{2}\pi$. For this case, the $O(1)$ core ϕ is $C_3 \lambda r^2 \sin(2\theta)$, so that the core velocities are

$$v_{xc} = -2C_3 \lambda x, \quad v_{yc} = 2C_3 \lambda y. \tag{25a, b}$$

Since $C_3 < 0$, there is core flow from the coldest positions to the hottest positions in order to complete the flow circuit for the flows inside the free-surface layer.

This research was supported by the US National Aeronautics and Space Administration under Cooperative Research Agreement NCC8-90 and by the US

National Science Foundation under Grant CTS 94-19484. Dr Frank Szofran of the NASA Marshall Space Flight Center and Dr Peter Dold of the University of Freiburg provided information about floating-zone crystal growth in ellipsoidal furnaces.

REFERENCES

Coriell, S. R. & Cordes, M. R. 1977 Theory of molten zone shape and stability. *J. Cryst. Growth* **42**, 466–472.

Croll, A., Dold, P. & Benz, K. W. 1994 Segregation in Si floating-zone crystals under microgravity and in a magnetic field. *J. Cryst. Growth* **137**, 95–101.

Hall, M. C. & Walker, J. S. 1993 Heat and mass transfer through a liquid metal in an infinitely long rotating cylinder with a uniform transverse magnetic field. *Intl J. Heat Mass Transfer* **36**, 3509–3514.

Hunt, J. C. R. & Ludford, G. S. S. 1968 Three-dimensional MHD duct flows with strong transverse magnetic fields. Part 1. Obstacles in a constant-area channel. *J. Fluid Mech.* **33**, 693–714.

Khine, Y. Y. & Walker, J. S. 1994 Thermocapillary convection in a cylinder with a strong non-uniform axisymmetric magnetic field. *J. Fluid Mech.* **276**, 369–388.

Lie, K. H., Walker, J. S. & Riahi, D. N. 1990 Free surface shape and AC electric current distribution for float zone silicon growth with a radio-frequency induction coil. *J. Cryst. Growth* **100**, 450–458.

Ma, N. & Walker, J. S. 1995 Liquid-metal buoyant convection in a vertical cylinder with a strong vertical magnetic field and with a non-axisymmetric temperature. *Phys Fluids* **7**, 2061–2071.

Morthland, T. E. & Walker, J. S. 1996 Thermocapillary convection during floating-zone silicon growth with a uniform or non-uniform magnetic field. *J. Cryst. Growth* **158**, 471–479.

Morthland, T. E. & Walker, J. S. 1997 Convective heat transfer due to thermocapillary convection with a strong magnetic field parallel to the free surface. *Intl J. Heat Mass Transfer* **40**, 3283–3291.

Muhlbauer, A., Erdmann, W. & Keller, W. 1983 Electrodynamic convection in silicon floating zones. *J. Cryst. Growth* **64**, 529–545.

Muller, G. & Rupp, R. 1991 The role of Marangoni convection in the growth of GaAs crystals by the floating zone technique under microgravity. *Cryst. Properties Preparation* **35**, 138–154.

Robertson, G. D. & O'Connor, D. 1986 Magnetic field effects on float-zone Si crystal growth. III. Strong axial fields. *J. Cryst. Growth* **76**, 111–122.

Rupp, R., Auerochs, S., Muller, G., Weyrich, C. & Leibenzeder, S. 1991 Growth of GaAs single crystals by the floating zone technique under microgravity. *Adv. Space Res.* **11** (7), 297–304.

Sabhapathy, P. & Salcudean, M. E. 1991 Numerical study of Czochralski growth of silicon in an axisymmetric magnetic field. *J. Cryst. Growth* **113**, 164–180.

Smith, M. C. & Davis, S. H. 1983 Instabilities of dynamic thermocapillary liquid layers. Part 1. Convective instabilities. *J. Fluid Mech.* **132**, 119–144.

Walker, J. S., Ludford, G. S. S. & Hunt, J. C. R. 1972 Three-dimensional MHD duct flows with strong transverse magnetic fields. Part 3. Variable-area rectangular ducts with insulating walls. *J. Fluid Mech.* **56**, 121–141.